





Stabilizer entropy dynamics after a quantum quench

Davide Rattacaso ^{1,2,3} Lorenzo Leone ⁴ Salvatore F. E. Oliviero ⁴ and Alioscia Hamma ^{3,5}

¹*Dipartimento di Fisica e Astronomia “G. Galilei”, Università degli Studi di Padova, Via Marzolo 8, I-35131, Padova, Italy*

²*INFN, Sezione di Padova, Via Marzolo 8, I-35131, Padova, Italy*

³*Dipartimento di Fisica “Ettore Pancini”, Università degli Studi di Napoli Federico II, Via Cintia 80126, Napoli, Italy*

⁴*Physics Department, University of Massachusetts Boston, Boston 02125, USA*

⁵*INFN, Sezione di Napoli, 80126 Napoli, Italy*



(Received 9 May 2023; accepted 18 September 2023; published 6 October 2023)

Stabilizer entropies (SE) measure deviations from stabilizer resources and as such are a fundamental ingredient for quantum advantage. In particular, the interplay of SE and entanglement is at the root of the complexity of classically simulating quantum many-body systems. In this paper, we study the dynamics of SE in a quantum many-body system away from the equilibrium after a quantum quench in an integrable system. We obtain two main results: (i) we show that SE, despite being an L -extensive quantity, equilibrates in a time that scales at most linearly with the subsystem size and (ii) we show that there is a SE length increasing linearly in time, akin to correlations and entanglement spreading.

DOI: [10.1103/PhysRevA.108.042407](https://doi.org/10.1103/PhysRevA.108.042407)

I. INTRODUCTION

In the past few decades, significant progress in quantum information science has been closely linked to efforts to synthesize artificial many-body systems. These devices can be used to simulate the quantum dynamics of large systems and execute algorithms with a potentially exponential advantage over classical computers [1–7]. Benchmarking the effectiveness of these devices as quantum systems, in other words, understanding their quantumness, involves identifying the resources that hinder its classical simulation. Entanglement has been viewed as the necessary ingredient for quantumness [8–10] since the discovery of the Bell inequalities and the first experimental demonstrations [11–14] and it plays a fundamental role in the hardness of simulating of quantum many-body systems, e.g., in tensor networks [15,16].

Beyond entanglement, however, resources outside the stabilizer formalism [17] are also necessary for complex behavior in quantum many-body systems [18–32]. Recently, stabilizer entropy (SE) [23] has emerged as a measure of nonstabilizerness in quantum systems. Being an entropy, the SE can be moved around subsystems, with the effect of purifying those from nonstabilizerness, and can give rise to phase transitions as shown [33,34]. Such a quantity can be experimentally measured on a quantum processor [35,36] and its direct computability makes it amenable for the study of quantum many-body systems [37–43].

The locality of interactions implies that in the gapped ground state of one-dimensional systems, there is a finite correlation length ξ such that the SE is localized [37,38] within a length $L_0 \sim \xi$, in the sense that SE can be extrapolated by subsystems of size L with an exponentially small error $O(e^{-L/L_0})$. On the other hand, for critical systems ξ , is found to diverge resulting in a power law for the approximation error.

In this paper, we investigate the behavior of SE in a quantum many-body system away from equilibrium after the

quantum quench of an integrable spin chain. The time profile of SE is computed analytically for all times. The two main results of this paper are (i) SE equilibrates to the value of the infinite time average following a transient period that increases at most linearly with the size of the subsystem, and (ii) the SE length increases ballistically and is upper bounded by a spreading velocity that is proportional to the Lieb-Robinson speed for the system [44].

The paper is organized as follows. First, in Sec. II we introduce the stabilizer entropy (SE) of a subsystem and investigate its evolution in the one-dimensional transverse field Ising model after a quench. We show that the SE equilibrates to the infinite time average and, after a large quench, the equilibration time of subsystem of size L scales as L/v_{LR} , where v_{LR} is the Lieb-Robinson speed associated to the quench. In Sec. III we introduce the notion of SE length. Looking at its time evolution, we can investigate how nonstabilizerness dynamically delocalizes: first, in Sec. III A, we use an analytical argument to show that the SE delocalizes in a light cone, then in Sec. III B we show that in the transverse-field Ising model (TFIM) this length grows ballistically with a speed proportional to the Lieb-Robinson velocity. Finally, Sec. IV is devoted to conclusions and future perspectives.

II. SE AWAY FROM EQUILIBRIUM

Let us start with the definition of SE [24]. Let ψ be a pure state of a system with N qubits on a chain and $\rho_L := \text{tr}_{N \setminus L} \psi$ its reduced density operator to a subsystem of L contiguous qubits. Denote \mathcal{P}_L the Pauli group on such a subsystem. The SE (of order two) of ρ_L is defined as

$$M_2(\rho_L) := -\log_2 W(\rho_L) - S_2(\rho_L), \quad (1)$$

where $W(\rho_L) := 2^{-L} \sum_{P \in \mathcal{P}_L} \text{tr}[(P\rho_L)^4]$ is the so-called *stabilizer purity* of ρ_L , while $S_2 = -\log_2 \text{Pur}(\rho_L)$ is 2-Rényi entanglement entropy of ρ_L and $\text{Pur}(\rho_L) \equiv \text{tr}(\rho_L^2)$. SE is a

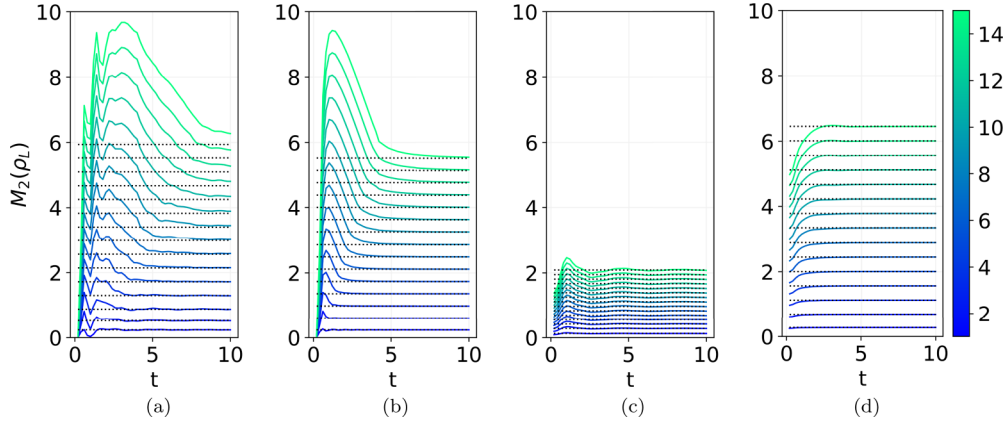


FIG. 1. Solid lines represent the time evolution of the SE M_2 [in Eq. (1)] of connected subsystems of different sizes L , ranging from 1 (blue lines below) to 15 (green lines above), after a quench of the transverse field λ in the Ising Hamiltonian in Eq. (2). Dotted black lines represent the SE of the corresponding dephased subsystems states $\bar{\psi}_L = \text{tr}_{N/L} \lim_{T \rightarrow \infty} T^{-1} \int_0^T \psi_t dt$. In (a) for the large quench $\lambda : 10^4 \rightarrow 0.5$; in (b) for the large critical quench $\lambda : 10^4 \rightarrow 1.0$; in (c) for the small quench $\lambda : 0.5 \rightarrow 0.6$; in (d) for the small critical quench $\lambda : 0.9 \rightarrow 1.0$. After a time transient, the SE equilibrates to the dephased state value, which is upper-bounded by $L/2$ as expected for an integrable dynamic.

good measure of nonstabilizerness from the point of view of resource theory. Indeed, it has the following properties: (i) faithfulness $M_\alpha(|\psi\rangle) = 0$ iff $|\psi\rangle$ is a stabilizer state, otherwise $M_\alpha(|\psi\rangle) > 0$, (ii) stability under Clifford operations: $\forall \Gamma \in \mathcal{C}_n$ we have that $M_\alpha(\Gamma|\psi\rangle) = M_\alpha(|\psi\rangle)$ and (iii) additivity $M_\alpha(|\psi\rangle \otimes |\phi\rangle) = M_\alpha(|\psi\rangle) + M_\alpha(|\phi\rangle)$ (the proof can be found in [24]). However, the SE with Rényi index $0 < \alpha < 2$ are shown to be nonmonotone under measurements followed by conditioned Clifford transformations, see [40].

Let us now turn our attention to the paradigmatic example of a family of *one*-parameter Hamiltonians: the *one*-dimensional TFIM $H_I(\lambda)$ defined as

$$H_I(\lambda) = - \sum_n (\sigma_n^x \sigma_{n+1}^x + \lambda \sigma_n^z), \quad (2)$$

with periodic boundary conditions $\sigma_{N+1} := \sigma_1$. In Eq. (2) σ_i^α for $\alpha = x, y, z$ are Pauli matrices acting on the i th spin and λ is the strength of the transverse field. The model is integrable for any value of λ using the Jordan-Wigner transformation and the Wick theorem [45–47]. Denote $|\psi_0(\lambda)\rangle$ the ground state of $H(\lambda)$. To study the dynamics of SE we subject the system to a quantum quench $H_I(\lambda) \mapsto H_I(\lambda')$ and let $|\psi_0(\lambda)\rangle$ evolve under the unitary evolution generated by $H(\lambda')$,

$$|\psi_0(\lambda)\rangle \mapsto |\psi_t(\lambda, \lambda')\rangle = e^{-iH(\lambda')t} |\psi_0(\lambda)\rangle. \quad (3)$$

Thanks to Wick's theorem, the time-dependent expectation values $P_t \equiv \text{tr}[P\psi_t(\lambda, \lambda')]$ can be computed analytically for any subsystem of length L in the thermodynamic limit $N \rightarrow \infty$ [48]. However, since there are 4^N such expectation values, we evaluate them for subsystems of sizes $L = 1, \dots, 16$.

In Fig. 1 we show the evolution of the SE of subsystems under different quenches $H(\lambda')$, and the SE $M_2(\bar{\rho}_L)$ of the dephased state $\bar{\rho}_L \equiv \text{tr}_{N/L} \sum_k \Pi_k(\lambda') \psi_0(\lambda) \Pi_k(\lambda') = \text{tr}_{N/L} \lim_{T \rightarrow \infty} T^{-1} \int_0^T \psi_t dt$. This is the infinite time average of the state, corresponding to the completely dephased state in the basis $\{\Pi_k(\lambda')\}$ of the Hamiltonian $H_I(\lambda')$ [49,50]. The initial state is chosen to be the completely polarized state for $\lambda \gg 1$, which is a stabilizer state so that $M_2(t=0) = 0$.

As we can see, there is a transient in which $M_2(t)$ increases rapidly before equilibrating to the SE of the dephased state. The equilibration is noteworthy because M_2 is an L -extensive quantity so it is not assured to equilibrate at finite t for every size L under general conditions [51–53].

For each configuration, the equilibration time τ can be defined as the time it takes for the subsystem's SE to reach the SE of the dephased state with fixed tolerance. The scaling of τ as a function of the system size is depicted in Fig. 2 for different quenches. Here we can see that, after a large quench, the equilibration time can be computed as $\tau \simeq L/v$ with $v \propto v_{LR}$, the Lieb-Robinson speed of propagation of signals reconstructed in Appendix C.

III. SE LENGTH DYNAMICS

The localization of SE in a quantum many-body system is described by the SE length. Localization of SE makes this quantity more amenable to computation in large systems. Indeed, although its computation does not involve a minimization procedure [19,22,54], it is still exponentially expensive as the number of Pauli operators P is 4^N , as we have seen in the previous section.

Recently, there has been an intensive effort for the characterization of systems for which SE can be computed efficiently [37–40]. In particular, for translationally invariant ground states of geometrically (gapped) local Hamiltonians [37], which can be well described by matrix product states (MPSs), and in general, for any MPS [38], there exists a constant L_0 , the *SE length*, such that for any $L > L_0$,

$$M_2(\rho_L) \simeq \alpha L + \beta, \quad (4)$$

up to a small additive error $\epsilon \ll \alpha L + \beta$. In Eq. (4) α, β , are constants that depend on the entire system state $|\psi\rangle$ [37] and therefore independent of the subsystem size L . The linearity of the SE is a consequence of the finite correlation length of the state [55]. More precisely (see Appendix A) the correction ϵ_L to the linear behavior in Eq. (4) scales as $\epsilon_L = \gamma e^{-L/\xi}$, where γ, ξ are constants depending on the finitely correlated state

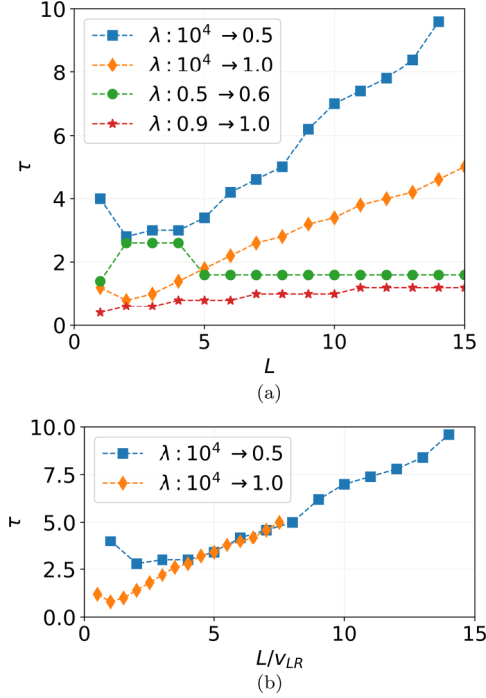


FIG. 2. In (a), the equilibration time (τ) for the subsystem's SE as a function of the number of sites (L) ranging from 0 to 15. Here the equilibration time is defined as the time it takes for the subsystem's SE to reach the SE of the dephased state with a tolerance of 5%. We consider four types of quenches: a large noncritical quench (represented by blue squares), a large critical quench (represented by yellow diamonds), a small noncritical quench (represented by green dots), and a small critical quench (represented by red stars). In (b) the number of sites is rescaled by the Lieb-Robinson speed. We can see that the equilibration time after a large quench scales as $\tau \simeq L/v$, where v_{LR} is the Lieb-Robinson speed of signals associated with the quench Hamiltonian and $v \propto v_{LR}$.

under consideration. Such behavior effectively defines the SE length being the constant L_0 such that $L_0 = \xi \log_2 \gamma / \epsilon$, for some tolerance $\epsilon \ll \alpha L_0 + \beta$.

The existence of a (finite) SE length L_0 makes SE easily computable for extended systems. To see this more concretely, consider a subsystem X of size L . From Eq. (4) we see that for $L > L_0 + 1$ and $\Delta \equiv M_2(\rho_{L_0+1}) - M_2(\rho_{L_0})$ one has

$$M_2(\rho_L) \simeq \Delta(L - L_0) + M_2(\rho_{L_0}), \quad (5)$$

which tells us that, once SE is measured for two subsystems of sizes L_0 and $L_0 + 1$ it can then be efficiently extrapolated, through Eq. (5), to a larger system sizes L . Note that it is crucial that $L > L_0$ to ensure the validity of Eq. (4) and thus of Eq. (5). The SE length L_0 quantifies both how nonstabilizerness is localized in the system and the effort needed to compute SE. As an example, in the ground state $|\psi_0(\lambda)\rangle$ of the TFIM, the SE length is $L_0 = 1$ for every $\lambda \gg 1$ and $\lambda \ll 1$ [37].

A. Nonstabilizerness delocalization

We have seen that after a quantum quench, M_2 equilibrates after a time scaling linearly with the size of the system. This

suggests that SE is spreading throughout the system. Such spreading should result in an increase in SE length. The main goal of this section is to show that the growth of the SE length L_t is upper bounded by an effective light cone.

We consider the case of states with finite correlation lengths. As it is well known, such states admit an efficient description by MPS [16]. Their time evolution under a local Hamiltonian $H(\lambda')$ results in a spreading of correlations [56] and increasing entropy of subsystems [57]. Both effects are encoded in the bond dimensions D for the MPS description, which increases at most as $D(t) \leq e^{A+vt}$ [58], where v is $O(1)$ in the system size. Using the fact that both the purity $\text{Pur}(\rho_L)$ and the stabilizer purity $W(\rho_L)$ can be written as an expectation value of a string of local observables on the replica state $|\psi \otimes \psi^*\rangle^{\otimes k}$ for $k = 1, 2$, respectively [38], we can show that the SE length L_t obeys the following bound:

$$L_t \leq L_0 + v_s t. \quad (6)$$

We refer to Appendix A for details. Here v_s is a constant that plays the role of an effective velocity and is $O(1)$ in the system size. The above equation shows that, under the evolution by a local Hamiltonian, SE delocalizes within an effective light cone constrained by the finite range of interactions in the quench Hamiltonian $H(\lambda')$.

B. SE length growth in the TFIM

In this subsection, we compute in the concrete case of TFIM the speed v_s for the SE length growth, that is, its delocalization. The behavior of the SE length L_t is dictated by the correction to the linear scaling in Eq. (4). Recall that Eq. (4) holds up to an additive error ϵ_{L_t} , where now L_t is a function of time $L_t \equiv L_0(t)$. The speed at which the error ϵ_{L_t} increases determines the velocity v_s of the spreading of L_t for $H_I(\lambda)$ [see Eq. (6)]. We thus numerically investigate the second derivative with respect to L of $M_2(\lambda, t) \equiv M_2[\rho_L^t(\lambda)]$, for $\rho_L^t(\lambda) = \text{tr}_{N \setminus L} |\psi_t(\lambda)\rangle\langle\psi_t(\lambda)|$ that, from Eq. (1), is a sum of two terms

$$\partial_L^2 M_2(\lambda, t) = \partial_L^2 T_4(\lambda, t) - \partial_L^2 T_2(\lambda, t), \quad (7)$$

where $T_4(\lambda, t) \equiv -\log_2 W[\rho_L^t(\lambda)] - L$, and $T_2(\lambda, t) \equiv S_2[\rho_L^t(\lambda)] - L$. Equation (7) tells us that the behavior of ϵ_{L_t} is, ultimately, determined by the fastest (in t) contribution between $\partial_L^2 T_2(\lambda, t)$ and $\partial_L^2 T_4(\lambda, t)$. Interestingly, the second term $\partial_L^2 T_2(\lambda, t)$ encodes the sublinear correction for the area law of MPSs for the 2-Rényi entropy of entanglement. In other words, the speed at which entanglement spread out in the system can be determined by only the behavior of $\partial_L^2 T_2(\lambda, t)$. On the other hand, the corrections to the nonstabilizerness additivity in Eq. (4) and their behavior after the quench are encoded in the evolution of both $\partial_L^2 T_4(\lambda, t)$ and $\partial_L^2 T_2(\lambda, t)$, which suggests a tight relationship between nonstabilizerness delocalization and entanglement growth. Indeed, through theoretical arguments, in Appendix A, we argue that nonstabilizerness could delocalize two times faster than entanglement. This consideration is found to be true by the numerical analysis below.

To extract the behavior of L_t and thus of the velocity v_s , we fix an error tolerance ϵ and define $l_{2,\epsilon}(t)$ and $l_{4,\epsilon}(t)$ as solutions of the following inequalities $|\partial_L^2 T_2| \leq \epsilon$, $|\partial_L^2 T_4| \leq \epsilon$

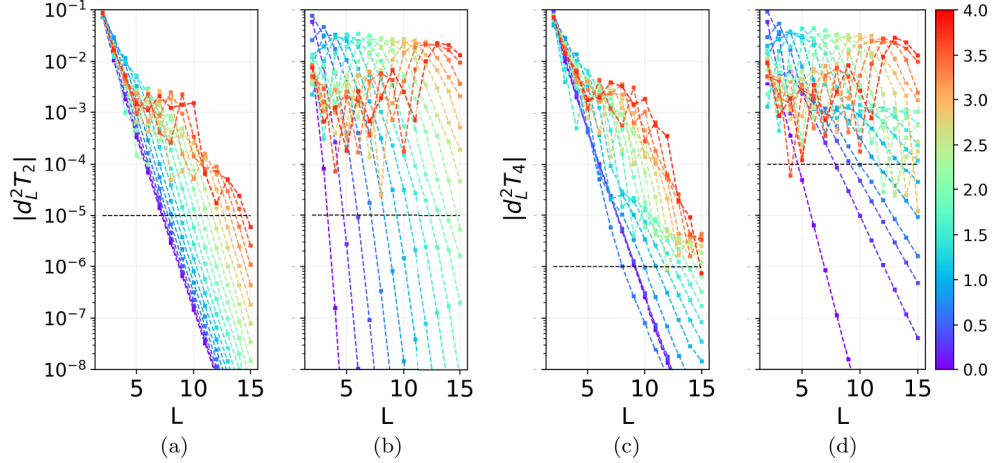


FIG. 3. Second space derivative of $T_2(\rho_L)$ and $T_4(\rho_L)$ [see Eq. (7)] as a function of the subsystem size L , ranging from 2 to 15, after the quench. Different lines represent different times in the range from 0 (purple line below) to 4 (red line above). The horizontal black line represents the error tolerance such that functions above the line decay exponentially. In (a) the second derivative of T_2 for the small quench $\lambda : 0.5 \rightarrow 0.6$. In (b) second derivative of T_2 for the large critical quench $\lambda : 10^4 \rightarrow 1.0$. In (c) the second derivative of T_4 for the small quench $\lambda : 0.5 \rightarrow 0.6$. In (d) the second derivative of T_4 for the large critical quench $\lambda : 10^4 \rightarrow 1.0$. All these derivatives can be upper-bounded by exponentially decaying functions: the SE additivity in Eq. (4) is preserved in time evolution with an exponentially small error for sufficient large subsystems.

definitively in time. Then we extract $v_s = \max\{v_{T_2}, v_{T_4}\}$ where $v_{T_k} \equiv \partial_t l_{k,\epsilon}$ for $k = 2, 4$. In Fig. 3 we depict the behavior of $|\partial_L^2 T_2(\lambda, t)|$ and $|\partial_L^2 T_4(\lambda, t)|$ for the quench protocols in which the definitive behavior is captured with the computational resources at our disposal, see also Appendix B. As expected, we observe that $|\partial_L^2 T_2(\lambda, t)|$ and $|\partial_L^2 T_4(\lambda, t)|$ decay exponentially below the dotted line representing the chosen

error tolerance ϵ . The associated lengths $l_{2,\epsilon}(t)$ and $l_{4,\epsilon}(t)$ as a function of t are shown in Fig. 4 for $t = 0, \dots, 4$: after an initial transient, both $l_{2,\epsilon}(t)$ and $l_{4,\epsilon}(t)$ grow ballistically. The associated velocities are $v_{T_2} \approx 2.5$ for $\lambda' = 0.5$ and $v_{T_2} \approx 5$ for $\lambda' \in \{1, 1.5, 2\}$, independently of the initial state; while $v_{T_4} \approx 5$ for $\lambda' = 0.5$ and $v_{T_4} \approx 10$ for $\lambda' = 2.0$. We conclude that, being $v_{T_4} > v_{T_2}$, $v_s \approx v_{T_4}$ and thus (compatibly with our theoretical considerations) the SE delocalizes two times faster than entanglement entropy.

Finally, we are going to show that the velocity v_s is proportional to the Lieb-Robinson speed v_{LR} . The Lieb-Robinson velocity associated with the Ising Hamiltonian can be reconstructed from the revivals after the quench. Revivals are brief detachments from the average value observables whose magnitude decays in time as the equilibration process nears completion. During these detachments, the system state gets briefly closer to the initial state. Therefore, revivals can be detected by looking at the Loschmidt echo (LE), that is, the squared fidelity between the evolved state and the initial state. The revival times T_{rev} are proportional to the system size N and are related to maximal group velocity in integrable systems, and therefore to the Lieb-Robinson speed in generic local systems, as $T_{\text{rev}} \approx N/(2v_{LR})$ [59]. The LE can be efficiently calculated for integrable spin chains in the fermionic representation described in [45]. In Appendix C we show that, independently of the initial state, Lieb-Robinson speed is $v_{LR} = 2$ for the paramagnetic quench $\lambda' > 1$, and $v_{LR} = 2\lambda'$ for the ferromagnetic quench $\lambda' < 1$. This result suggests a proportionality relation between v_s and v_{LR} .

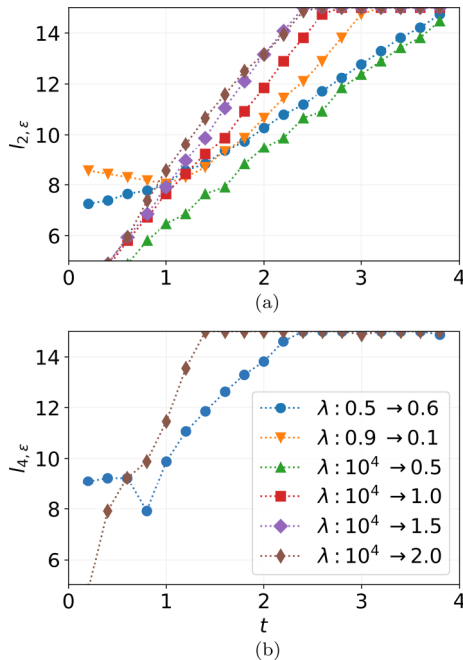


FIG. 4. Evolution of the localization lengths $l_{2,\epsilon}$ and $l_{4,\epsilon}$ such that $|\partial_L^2 T_2| \leq \epsilon$, $|\partial_L^2 T_4| \leq \epsilon$, for different quench protocols and time ranging from 0 to 4. We consider large quenches from $\lambda \gg 1$ and small quenches $\lambda' = \lambda + 0.1$. Quenches to $\lambda = 1.0$ are critical. The spreading is ballistic and defines a light cone.

IV. CONCLUSION

In this work, we studied the behavior away from equilibrium of the nonstabilizer properties of a quantum many-body system after a sudden quench. The system studied is the integrable quantum Ising chain, which allowed for a

thoroughly analytical treatment, and nonstabilizerness is computed through the stabilizer Rényi entropy M_2 . Two main results are found. (i) M_2 increases and finally equilibrates in a time proportional to the system size and (ii) one can define a stabilizer entropy *length* L_t that describes the SE localization [37]. Such length increases linearly in time showing that M_2 spreads ballistically through the system until complete delocalization.

In perspective, this work calls for several questions. In [33,60–64] it was shown that the onset of quantum chaotic behavior in quantum circuits corresponds to a value of $M_2 > N/2$, and full-fledged quantum chaos is attained near-maximal values for SE. Of course, chaos in quantum circuits is not the same than chaos in Hamiltonian systems, being defined there as the onset of universal entanglement features or universal behavior of the OTOCs [60]. However, our results show that the equilibrium value of SE for the integrable quantum quench is below the quantum chaotic threshold of quantum circuits. This fact raises the question whether the equilibrium SE is a tell-tale of the onset of quantum chaos in the Hamiltonians system. We indeed speculate that a non-integrable system will equilibrate to a larger value for M_2 . It would be intriguing if the increase in equilibrium SE compared to the integrable case would depend on the strength of the interability breaking term.

Second, preliminary numerical analysis suggests that subtle features of SE dynamics may be erased by the operation of partial trace. This is akin to the problem of presence of thermal fluctuations when evaluating entanglement. A possible strategy would be to localize SE in a subsystem by measurements in a Clifford basis (e.g., the computational basis) and evaluate the local residual SE in the pure state. This would entail averaging over all the possible Clifford measurements.

Third, the onset of quantum chaos depends on the interplay between both entanglement and SE [60–72], and it is still an open question to what extent they are sufficient and/or necessary. Recently [41], it was shown that the flatness of the entanglement spectrum of a subsystem is a good probe for SE. Since it is also a probe for entanglement, it is tempting to study the dynamics of flatness to probe the onset of quantum chaos.

Finally, finite-size scaling in L for larger sizes would allow for a reliable analysis of the temporal fluctuations. To this end, we plan to employ Monte Carlo methods to sample SE efficiently. Finally, we remark on the fascinating relationship between SE and the bond dimension D . The study of the interplay of SE with the efficiency of tensor network methods is thus potentially of great importance for the issue of simulating quantum many-body systems on a classical computer.

ACKNOWLEDGMENTS

The authors acknowledge important discussions with R. Fazio, P. Lucignano, and J. Odavic. A.H. was supported by the PNRR MUR Project No. PE0000023-NQSTI and PNRR MUR Project No. CN 00000013-ICSC. L.L. and S.O. acknowledge support from NSF Award No. 2014000. D.R. acknowledges support from the EU project EURyQA.

APPENDIX A: PROOF EQ. (6)

First of all, let us define the functions $T_4(\lambda, t) \equiv -\log W(\rho_L^t(\lambda)) - L$, and $T_2(\lambda, t) \equiv S_2[\rho_L^t(\lambda)] - L$. In terms of T_2 and T_4 , the SE can be written as

$$M_2(\lambda, t) = T_4(\lambda, t) - T_2(\lambda, t). \tag{A1}$$

As shown in [38], 2^{T_2} and 2^{T_4} are expectation values of strings of L connected observables on replica states. More precisely, define $|\psi^{(k)}\rangle \equiv |(\psi \otimes \psi^*)^{\otimes k}\rangle$ for $k = 1, 2$. Define the local observable $A_i^{(k)} = \mathbb{I}_i^{\otimes 2k} + \sum_{\alpha=1}^3 (\sigma_i^\alpha \otimes \sigma_i^{\alpha*})^{\otimes k}$ for $k = 1, 2$ and σ_i^α for $\alpha = x, y, z$ being single-qubit Pauli matrices. Then $2^{T_{2k}(\lambda, t)}$ for $k = 1, 2$ can be recast as

$$2^{T_{2k}(\lambda, t)} = \langle \psi^{(k)} | A_1^{(k)} \otimes \dots \otimes A_L^{(k)} \otimes \mathbb{I}_{N \setminus L} | \psi^{(k)} \rangle. \tag{A2}$$

To explain the behavior of the SE under time evolution and its relation to the locality, we want to understand how strings of observables behave in a state with finite correlation length, and how they change while, after a quantum quench, correlations spread out in the system.

We start by looking at the initial translationally invariant state $|\psi(0)\rangle$. Having a finite correlation length, this can be represented as an MPS with polynomial bond dimension D . Similarly, $|\psi^{(k)}\rangle$ for $k = 1, 2$ is a MPS state with bond dimension $D_k = D^{2k}$. Let $\tau_{\psi^{(k)}}$ be the transfer matrix of the MPS and $\tau_{\psi^{(k)}, A}$ be the transfer matrix of the MPS contracted with the local operator A . The expectation value of a string of local operators $A_i^{(k)}$ can be written as

$$\langle \psi^{(k)} | A_1^{(k)} \otimes \dots \otimes A_L^{(k)} \otimes \mathbb{I}_{N \setminus L} | \psi^{(k)} \rangle = \lim_{N \rightarrow \infty} \text{tr}(\tau_{\psi^{(k)}}^{N-L} \tau_{\psi^{(k)}, A}^L). \tag{A3}$$

Now, we call $|R_{\psi^{(k)}}^{(i)}\rangle$ and $|L_{\psi^{(k)}}^{(i)}\rangle$ the right and left eigenvectors of $\tau_{\psi^{(k)}}$ and $\lambda_{\psi^{(k)}}^{(i)}$ the associated eigenvalues. In this way, the transfer matrix can be written as

$$\tau_{\psi^{(k)}} = \sum_{i=1}^{D_k^2} \lambda_{\psi^{(k)}}^{(i)} |R_{\psi^{(k)}}^{(i)}\rangle \langle L_{\psi^{(k)}}^{(i)}|, \tag{A4}$$

where $|\lambda_{\psi^{(k)}}^{(i)}| > |\lambda_{\psi^{(k)}}^{(i+1)}|$, and $\lambda_{\psi^{(k)}}^{(1)} = 1$ for the normalization condition. Analogously, we can write

$$\tau_{\psi^{(k)}, A} = \sum_{i=1}^{D_k^2} \lambda_{\psi^{(k)}, A}^{(i)} |R_{\psi^{(k)}, A}^{(i)}\rangle \langle L_{\psi^{(k)}, A}^{(i)}|, \tag{A5}$$

with $|\lambda_{\psi^{(k)}, A}^{(i)}| > |\lambda_{\psi^{(k)}, A}^{(i+1)}|$. The eventual degeneration of eigenvalues does not affect the general behavior of this proof. Hence, a string expectation value can be written as

$$\begin{aligned} & \langle \psi^{(k)} | A_1^{(k)} \otimes \dots \otimes A_L^{(k)} \otimes \mathbb{I}_{N \setminus L} | \psi^{(k)} \rangle \\ &= \sum_{i=1}^{D_k^2} (\lambda_{\psi^{(k)}, A}^{(i)})^L \langle L_{\psi^{(k)}}^{(i)} | R_{\psi^{(k)}, A}^{(i)} \rangle \langle L_{\psi^{(k)}, A}^{(i)} | R_{\psi^{(k)}}^{(i)} \rangle. \end{aligned} \tag{A6}$$

At this point, we define

$$2^{m(\psi^{(k)})} := \lambda_{\psi^{(k)}, A}^{(1)}, \tag{A7}$$

$$2^{q(\psi^{(k)})} := \langle L_{\psi^{(k)}}^{(1)} | R_{\psi^{(k)}, A}^{(1)} \rangle \langle L_{\psi^{(k)}, A}^{(1)} | R_{\psi^{(k)}}^{(1)} \rangle, \tag{A8}$$

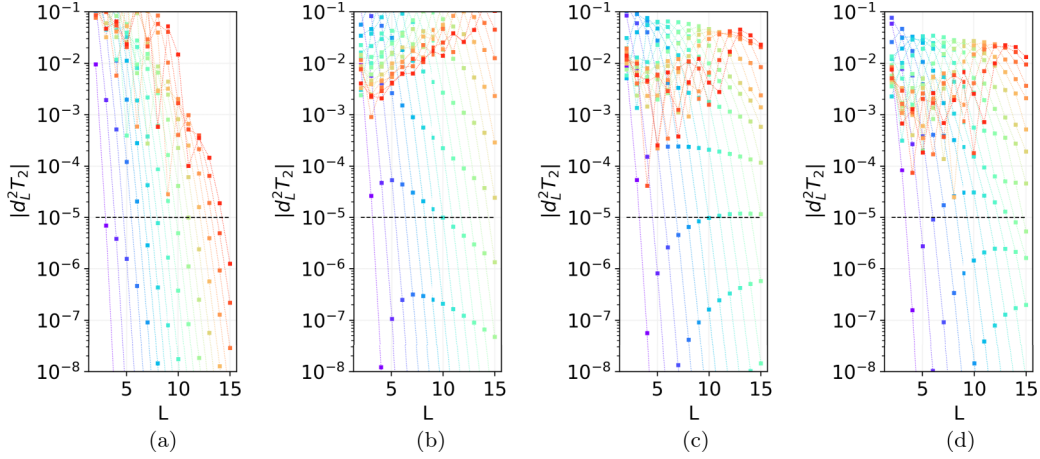


FIG. 5. Second space derivative of $T_2(\rho_L)$ as a function of the subsystem size L after a quench from $\lambda = 10^4$ to different values of λ' . The subsystem size goes from 2 to 15. Different lines represent different times in the range from 0 (purple line below) to 4 (red line above). The horizontal black line represents the error tolerance such that functions above the line are definitively exponential. In (a) $\lambda' = 0.5$; in (b) $\lambda' = 1.0$ (critical quench); in (c) $\lambda' = 1.5$; in (d) $\lambda' = 2.0$.

$$e^{-1/\xi(\psi^{(k)})} := \left| \frac{\lambda_{\psi^{(k),A}}^{(2)}}{\lambda_{\psi^{(k),A}}^{(1)}} \right|, \quad (\text{A9})$$

$$F(\psi^{(k)}) := \left| \frac{\langle L_{\psi^{(k)}}^{(2)} | R_{\psi^{(k),A}}^{(2)} \rangle \langle L_{\psi^{(k),A}}^{(2)} | R_{\psi^{(k)}}^{(2)} \rangle}{\langle L_{\psi^{(k)}}^{(1)} | R_{\psi^{(k),A}}^{(1)} \rangle \langle L_{\psi^{(k),A}}^{(1)} | R_{\psi^{(k)}}^{(1)} \rangle} \right|. \quad (\text{A10})$$

Since $|\lambda_{\psi^{(k),A}}^{(i)}|^L \gg |\lambda_{\psi^{(k),A}}^{(i+1)}|^L$, for sufficiently large L we obtain

$$\begin{aligned} & \langle \psi^{(k)} | A_1^{(k)} \otimes \cdots \otimes A_L^{(k)} \otimes \mathbb{1}_{N \setminus L} | \psi^{(k)} \rangle \\ &= 2^{m(\psi^{(k)})L + q(\psi^{(k)})} (1 + \varepsilon^{(k)}), \end{aligned} \quad (\text{A11})$$

where

$$|\varepsilon^{(k)}| \leq D_k^2 e^{-L/\xi(\psi^{(k)})} F(\psi^{(k)}) \ll 1. \quad (\text{A12})$$

It should be noted that the derivation of this bound assumes that $F(\psi^{(k)})$ is finite. In the event that this condition is not met, an equivalent derivation can be obtained by considering the next eigenvalue $\lambda_{\psi^{(k),A}}^{(2)}$. In this case,

$$\begin{aligned} F(\psi_k) &:= \left| \langle L_{\psi^{(k)}}^{(3)} | R_{\psi^{(k),A}}^{(3)} \rangle \langle L_{\psi^{(k),A}}^{(3)} | R_{\psi^{(k)}}^{(3)} \rangle \right| / \\ & \left| \langle L_{\psi^{(k)}}^{(2)} | R_{\psi^{(k),A}}^{(2)} \rangle \langle L_{\psi^{(k),A}}^{(2)} | R_{\psi^{(k)}}^{(2)} \rangle \right|, \end{aligned}$$

and the linear approximation is preserved with the same exponential correction.

With this formalism, also the effect of locality on time evolution can be easily addressed. When an MPS evolves with a local Hamiltonian $H(\lambda')$, the spreading of correlations [56] and the increasing entropy of subsystems [57] are encoded in the bond dimensions, which increases at most as $D(t) \leq e^{A+vt}$ [58], where v is $O(1)$ in the system size. We can then generalize the result obtained in Eq. (A11) in the following

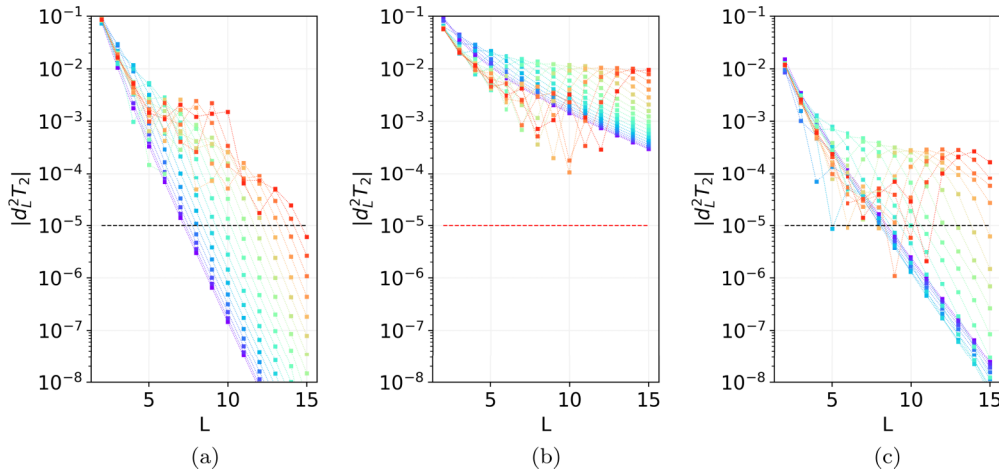


FIG. 6. Second space derivative of $T_2(\rho_L)$ as a function of the subsystem size L after a quench from λ to different values of $\lambda' = \lambda + 0.1$. The subsystem size goes from 2 to 15. Different lines represent different times in the range from 0 (purple line below) to 4 (red line above). The horizontal black line represents the error tolerance such that functions above the line are definitively exponential. In (a) $\lambda = 0.5$; in (b) $\lambda = 0.9$ (critical quench); in (c) $\lambda = 1.5$.

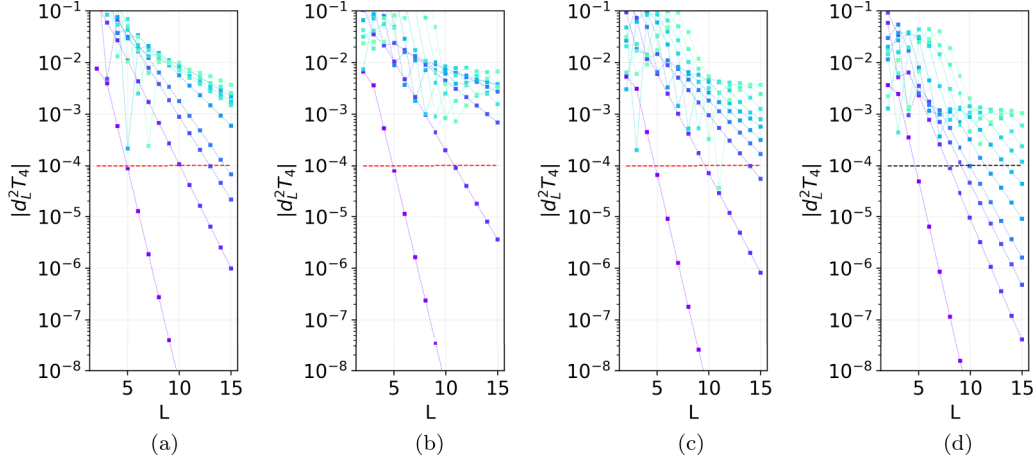


FIG. 7. Second space derivative of $T_4(\rho_L)$ as a function of the subsystem size L after a quench from $\lambda = 10^4$ to different values of λ' . The subsystem size goes from 2 to 15. Different lines represent different times in the range from 0 (purple line below) to 4 (red line above). The horizontal black line represents the error tolerance such that functions above the line are definitively exponential. In (a) $\lambda' = 0.5$; in (b) $\lambda' = 1.0$ (critical quench); in (c) $\lambda' = 1.5$; in (d) $\lambda' = 2.0$.

way:

$$\begin{aligned} \langle \psi^{(k)}(t) | A_1^{(k)} \otimes \dots \otimes A_L^{(k)} \otimes \mathbb{I}_{N \setminus L} | \psi^{(k)} \rangle \\ = 2^{m(\psi^{(k)}(t))L + q(\psi^{(k)}(t))} (1 + \varepsilon^{(k)}), \end{aligned} \quad (\text{A13})$$

where we defined $|\psi^{(k)}(t)\rangle \equiv [U_t \otimes U_t^*]^{\otimes k} |\psi^{(k)}\rangle$ with $U_t = e^{-iH(\lambda')t}$. Consequently, $\varepsilon^{(k)}$ is now bounded for sufficiently large L as

$$|\varepsilon^{(k)}| \leq e^{4kA + 4kvt} e^{-L/\xi(\psi^{(k)}(t))} F(\psi^{(k)}(t)) \ll 1, \quad (\text{A14})$$

where we used that $D_k = D^{2k}$ and consequently that $D_k(t) = D(t)^{2k} \leq e^{2kA + 2kvt}$. At this point we define $\varepsilon_0^{(k)} = e^{4kA} \max_t F[\psi^{(k)}(t)]$ and $\chi^{(k)} = \max_t \xi[\psi^{(k)}(t)]$. We obtain that

$$|\varepsilon^{(k)}| \leq \varepsilon_0^{(k)} e^{(4kv\chi^{(k)}t - L)/\chi^{(k)}}. \quad (\text{A15})$$

With this result, let us focus on the behavior of the SE $M_2 = T_4 - T_2$. Since 2^{T_2} and 2^{T_4} are equal to

$$\begin{aligned} T_2 &= m[\psi^{(1)}(t)]L + q[\psi^{(1)}(t)] + \varepsilon^{(1)}, \\ T_4 &= m[\psi^{(2)}(t)]L + q[\psi^{(2)}(t)] + \varepsilon^{(2)}, \end{aligned}$$

$$|\varepsilon^{(1)}| \leq \varepsilon_0^{(1)} e^{(4v\chi^{(1)}t - L)/\chi^{(1)}},$$

$$|\varepsilon^{(2)}| \leq \varepsilon_0^{(2)} e^{(8v\chi^{(2)}t - L)/\chi^{(2)}}. \quad (\text{A16})$$

It follows that

$$\begin{aligned} M_2(\rho_L) &= \{m[\psi^{(2)}(t)] - m[\psi^{(1)}(t)]\}L \\ &\quad + \{q[\psi^{(2)}(t)] - q[\psi^{(1)}(t)]\} + \varepsilon_M \end{aligned}$$

$$|\varepsilon_M| \leq 2 \max\{\varepsilon^{(1)}, \varepsilon^{(2)}\}. \quad (\text{A17})$$

In a nutshell, during time evolution corrections to the linearity of nonstabilizerness are exponentially small out from a light

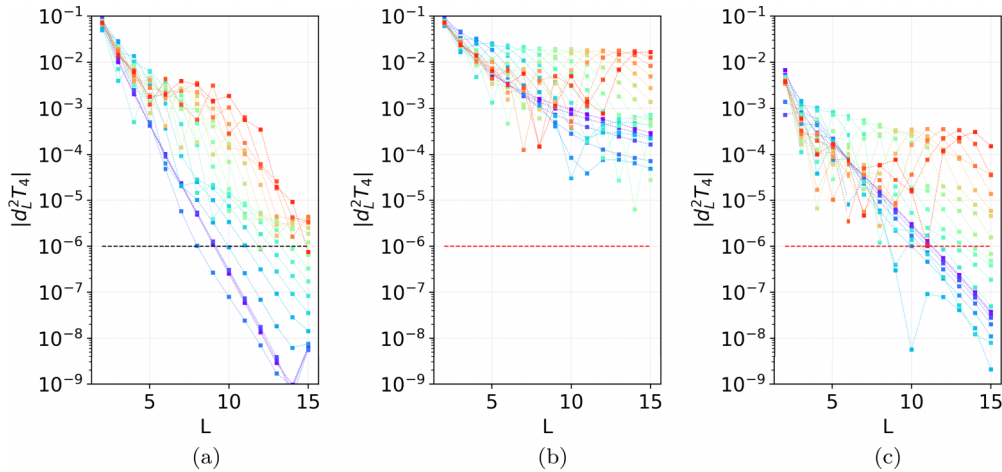


FIG. 8. Second space derivative of $T_4(\rho_L)$ as a function of the subsystem size L after a quench from λ to different values of $\lambda' = \lambda + 0.1$. The subsystem size goes from 2 to 15. Different lines represent different times in the range from 0 (purple line below) to 4 (red line above). The horizontal black line represents the error tolerance such that functions above the line are definitively exponential. In (a) $\lambda = 0.5$; in (b) $\lambda = 0.9$ (critical quench); in (c) $\lambda = 1.5$.

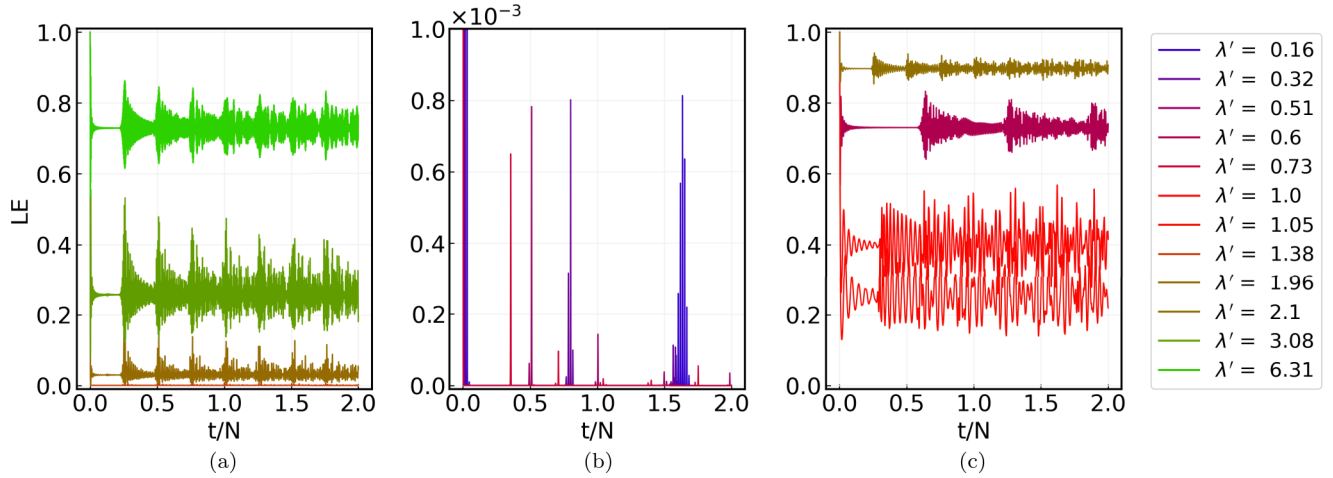


FIG. 9. Evolution of the LE with respect to the rescaled time t/N , where t runs from 0 to $2N$. In (a,b) for the large quench protocol where the initial state is $|\psi\rangle \approx |\uparrow \dots \uparrow\rangle$, for a system of $N = 100$ spins. In (c) for the small quench protocol where $\lambda' = \lambda + 0.1$, for a system of $N = 200$ spins.

cone. The speed at which the exponential bound increases determines the light cone in which the SE spreads out. To figure this out, we fix an error tolerance ϵ and we find the values $L_{2,\epsilon}$ and $L_{4,\epsilon}$ such that $|\varepsilon^{(1)}| \leq \epsilon$ and $|\varepsilon^{(2)}| \leq \epsilon$ definitively as a consequence of the previous bound. The SE length L_t is $\max\{L_{2,\epsilon}, L_{4,\epsilon}\}$.

Taking into account Eqs. (A16) $L_{2,\epsilon}$ and $L_{4,\epsilon}$ increases at most as

$$\begin{aligned} L_{2,\epsilon} &= \xi[\psi^{(1)}(t)] \log_2(\varepsilon_0^{(1)}/\epsilon) + 4v\chi^{(1)}t, \\ L_{4,\epsilon} &= \xi[\psi^{(2)}(t)] \log_2(\varepsilon_0^{(2)}/\epsilon) + 8v\chi^{(2)}t. \end{aligned} \quad (\text{A18})$$

Therefore, we can conclude that

$$L_t \leq L_0 + v_s t, \quad (\text{A19})$$

where $v_s = \max\{4v\chi^{(1)}, 8v\chi^{(2)}\}$ is $O(1)$ in the system size. Remarkably, when $\chi^{(1)}$ is comparable with $\chi^{(2)}$, the error on T_4 spreads two times faster than the error on T_2 .

APPENDIX B: ADDITIONAL NUMERICAL DATA

In Figs. 5 and 6, we show the exponential decay of the correction to the linear behavior of T_2 , encoded in the second space derivative, after different quenches. Analogously,

in Figs. 7 and 8 we represent the exponential decay of the correction to the linear behavior of T_4 .

In each figure, we can see that the exponential behavior is definitive for a sufficiently large system, as predicted in Appendix A. The size of this large system depends on time and on the quench protocol. Therefore, capturing the definitive behavior is not always possible with our computational resources. When the definitive behavior of the derivative is not captured by our data [e.g. Fig. 6(b)] the dashed line is red, otherwise it is black. In this later case, we observe that the derivative decays definitively exponentially below the dotted line.

APPENDIX C: LIEB-ROBINSON SPEED

In this Appendix, we analyze the revivals in the Ising model after a quantum quench to reconstruct the associated Lieb-Robinson speed.

In Fig. 9 we plot the LE evolution as a function of the rescaled time t/N , after the large quench, in Figs. 9(a) and 9(b), and a large quench, in Fig. 9(c). The revival time is $T_{\text{rev}} \approx N/4$ for $\lambda' > 1$, and $T_{\text{rev}} \approx N/(\lambda'/4)$ for $\lambda' < 1$. Therefore, the associated velocity is $v_{\text{LR}} = 2$ for $\lambda' > 1$, and $v_{\text{LR}} = 2\lambda'$ for $\lambda' < 1$. As expected from the fact that the Lieb-Robinson velocity only depends on the quench Hamiltonian, the same behavior is encountered both in the small quench and in the large quench.

[1] D. Deutsch and R. Jozsa, *Proc. R. Soc. London, Ser. A* **439**, 553 (1992).
 [2] P. Shor, in *Proceedings 35th Annual Symposium on Foundations of Computer Science* (ACM, New York, 1994), pp. 124–134.
 [3] S. Lloyd, *Science* **273**, 1073 (1996).
 [4] L. K. Grover, *A Fast Quantum Mechanical Algorithm for Database Search* (Association for Computing Machinery, New York, 1996), pp. 212–219.
 [5] A. Y. Kitaev, *Russ. Math. Surv.* **52**, 1191 (1997).

[6] D. S. Abrams and S. Lloyd, *Phys. Rev. Lett.* **83**, 5162 (1999).
 [7] A. W. Harrow, A. Hassidim, and S. Lloyd, *Phys. Rev. Lett.* **103**, 150502 (2009).
 [8] A. Aspect, P. Grangier, and G. Roger, *Phys. Rev. Lett.* **47**, 460 (1981).
 [9] A. Aspect, P. Grangier, and G. Roger, *Phys. Rev. Lett.* **49**, 91 (1982).
 [10] A. Aspect, J. Dalibard, and G. Roger, *Phys. Rev. Lett.* **49**, 1804 (1982).

- [11] J. S. Bell, *Phys. Phys. Fiz.* **1**, 195 (1964).
- [12] A. Fine, *Phys. Rev. Lett.* **48**, 291 (1982).
- [13] B. M. Terhal, *Phys. Lett. A* **271**, 319 (2000).
- [14] R. F. Werner and M. M. Wolf, [arXiv:quant-ph/0107093](https://arxiv.org/abs/quant-ph/0107093).
- [15] J. I. Latorre, E. Rico, and G. Vidal, *Quant. Inf. Comput.* **4**, 48 (2004).
- [16] R. Orús, *Ann. Phys. (NY)* **349**, 117 (2014).
- [17] D. Gottesman, *Group22: Proceedings of the XXII International Colloquium on Group Theoretical Methods in Physics*, edited by S. P. Corney, R. Delbourgo, and P. D. Jarvis (International Press, Cambridge, MA, 1999), pp. 32–43.
- [18] S. Bravyi and A. Kitaev, *Phys. Rev. A* **71**, 022316 (2005).
- [19] E. T. Campbell and D. E. Browne, *Phys. Rev. Lett.* **104**, 030503 (2010).
- [20] E. T. Campbell and M. Howard, *Phys. Rev. A* **95**, 022316 (2017).
- [21] M. Howard and E. Campbell, *Phys. Rev. Lett.* **118**, 090501 (2017).
- [22] J. R. Seddon and E. T. Campbell, *Proc. R. Soc. A* **475**, 20190251 (2019).
- [23] L. Leone, S. F. E. Oliviero, and A. Hamma, *Phys. Rev. Lett.* **128**, 050402 (2022).
- [24] L. Leone, S. F. E. Oliviero, and A. Hamma, *Phys. Rev. A* **107**, 022429 (2023).
- [25] C. Chamon, A. Hamma, and E. R. Mucciolo, *Phys. Rev. Lett.* **112**, 240501 (2014).
- [26] Z.-C. Yang, A. Hamma, S. M. Giampaolo, E. R. Mucciolo, and C. Chamon, *Phys. Rev. B* **96**, 020408(R) (2017).
- [27] S. Zhou, Z.-C. Yang, A. Hamma, and C. Chamon, *SciPost Phys.* **9**, 087 (2020).
- [28] Z.-W. Liu and A. Winter, *PRX Quantum* **3**, 020333 (2022).
- [29] C. D. White, C. J. Cao, and B. Swingle, *Phys. Rev. B* **103**, 075145 (2021).
- [30] T. J. Sewell and C. D. White, *Phys. Rev. B* **106**, 125130 (2022).
- [31] N. Koukoulekidis and D. Jennings, *npj Quantum Inf.* **8**, 42 (2022).
- [32] M. Hinsche, M. Ioannou, A. Nietner, J. Haferkamp, Y. Quek, D. Hangleiter, J.-P. Seifert, J. Eisert, and R. Sweke, *Phys. Rev. Lett.* **130**, 240602 (2023).
- [33] L. Leone, S. F. E. Oliviero, G. Esposito, and A. Hamma, [arXiv:2302.07895](https://arxiv.org/abs/2302.07895).
- [34] P. Niroula, C. D. White, Q. Wang, S. Johri, D. Zhu, C. Monroe, C. Noel, and M. J. Gullans, [arXiv:2304.10481](https://arxiv.org/abs/2304.10481).
- [35] S. F. E. Oliviero, L. Leone, A. Hamma, and S. Lloyd, *npj Quantum Inf.* **8**, 148 (2022).
- [36] T. Haug and M. S. Kim, *PRX Quantum* **4**, 010301 (2023).
- [37] S. F. E. Oliviero, L. Leone, and A. Hamma, *Phys. Rev. A* **106**, 042426 (2022).
- [38] T. Haug and L. Piroli, *Phys. Rev. B* **107**, 035148 (2023).
- [39] G. Lami and M. Collura, [arXiv:2303.05536](https://arxiv.org/abs/2303.05536).
- [40] T. Haug and L. Piroli, *Quantum* **7**, 1092 (2023).
- [41] E. Tirrito, P. S. Tarabunga, G. Lami, T. Chanda, L. Leone, S. F. E. Oliviero, M. Dalmonte, M. Collura, and A. Hamma, [arXiv:2304.01175](https://arxiv.org/abs/2304.01175).
- [42] J. Odavić, T. Haug, G. Torre, A. Hamma, F. Franchini, and S. M. Giampaolo, *SciPost Phys.* **15**, 131 (2023).
- [43] L. Chen, R. J. Garcia, K. Bu, and A. Jaffe, [arXiv:2211.10350](https://arxiv.org/abs/2211.10350).
- [44] E. H. Lieb and D. W. Robinson, *Commun. Math. Phys.* **28**, 251 (1972).
- [45] E. Lieb, T. Schultz, and D. Mattis, *Ann. Phys.* **16**, 407 (1961).
- [46] P. Pfeuty, *Ann. Phys. (NY)* **57**, 79 (1970).
- [47] E. Barouch and B. M. McCoy, *Phys. Rev. A* **3**, 786 (1971).
- [48] G. B. Mbeng, A. Russomanno, and G. E. Santoro, [arXiv:2009.09208](https://arxiv.org/abs/2009.09208).
- [49] M. Rigol, V. Dunjko, and M. Olshanii, *Nature (London)* **452**, 854 (2008).
- [50] J. Eisert, M. Friesdorf, and C. Gogolin, *Nat. Phys.* **11**, 124 (2015).
- [51] H. Tasaki, *Phys. Rev. Lett.* **80**, 1373 (1998).
- [52] P. Reimann, *Phys. Rev. Lett.* **101**, 190403 (2008).
- [53] N. Linden, S. Popescu, A. J. Short, and A. Winter, *Phys. Rev. E* **79**, 061103 (2009).
- [54] E. T. Campbell, B. M. Terhal, and C. Vuillot, *Nature (London)* **549**, 172 (2017).
- [55] M. B. Hastings and T. Koma, *Commun. Math. Phys.* **265**, 781 (2006).
- [56] B. Nachtergaele, Y. Ogata, and R. Sims, *J. Stat. Phys.* **124**, 1 (2006).
- [57] J. Eisert, *Modeling and Simulation* **3**, 520 (2013).
- [58] A. M. Alhambra and J. I. Cirac, *PRX Quantum* **2**, 040331 (2021).
- [59] J. Häppölä, G. B. Halász, and A. Hamma, *Phys. Rev. A* **85**, 032114 (2012).
- [60] L. Leone, S. F. E. Oliviero, Y. Zhou, and A. Hamma, *Quantum* **5**, 453 (2021).
- [61] S. F. E. Oliviero, L. Leone, and A. Hamma, *Phys. Lett. A* **418**, 127721 (2021).
- [62] S. F. E. Oliviero, L. Leone, S. Lloyd, and A. Hamma, [arXiv:2212.11337](https://arxiv.org/abs/2212.11337).
- [63] L. Leone, S. F. E. Oliviero, S. Lloyd, and A. Hamma, [arXiv:2212.11338](https://arxiv.org/abs/2212.11338).
- [64] L. Leone, S. F. E. Oliviero, S. Piemontese, S. True, and A. Hamma, *Phys. Rev. A* **106**, 062434 (2022).
- [65] N. Dowling, P. Kos, and K. Modi, [arXiv:2304.07319](https://arxiv.org/abs/2304.07319).
- [66] L. Leone, S. F. E. Oliviero, and A. Hamma, *Entropy* **23**, 1073 (2021).
- [67] S. F. E. Oliviero, L. Leone, F. Caravelli, and A. Hamma, *SciPost Phys.* **10**, 076 (2021).
- [68] N. Dowling and K. Modi, [arXiv:2210.14926](https://arxiv.org/abs/2210.14926).
- [69] S. Omanakuttan, K. Chinni, P. D. Blocher, and P. M. Poggi, *Phys. Rev. A* **107**, 032418 (2023).
- [70] K. Goto, T. Nosaka, and M. Nozaki, *Phys. Rev. D* **106**, 126009 (2022).
- [71] S. True and A. Hamma, *Quantum* **6**, 818 (2022).
- [72] J. Kim, Y. Oz, and D. Rosa, *J. Stat. Mech.* (2023) 023104.